Lab #2

Magnetic Levitation System

MECHENG 552

Team 4B

Saptadeep Debnath
Manavendra Desai
Ellen Kim
David Radtke

Professor Shorya Awtar
04 October 2019

Department of Mechanical Engineering
University of Michigan, Ann Arbor

Contents

List of Figures

List of Tables

1 Overall System Modeling (21pts)

(a) Assumptions (7)

- Plant
  - Feedback loop of the op amp creates no significant dynamics
    - Reasonable: The bandwidth of an op amp is considerably higher than the bandwidth of the other parts of the system
    - Violations to Assumption: The input into the op amp loop is of a frequency near or above the bandwidth of the op amp
  - The relationship between current and position of is proportional by an invariant constant 'C'
    - Reasonable: C is the consequence of the geometry and material choices that constitute the system, which should not change over time.
    - Violations to Assumption:
      - The attraction between the ball and the actuator does not become zero when current is 0 because of the effect of remanence, but this effect is small enough to ignore.
      - As time goes on, the resistive components can heat up and become more resistive. This violation should not be met as long as the system is not run for too long.
  - The relationship between the input voltage and desired current can be related by a ratio of the input and sense resistors.
    - Reasonable: Like previously stated, our op amp should meet the Golden Rules which subsequently allows us to derive this outcome.
    - Violation to Assumption: The Golden Rules are not aligned perfectly with reality and so the ratio will not be perfect in reality.
  - We linearize the relationship between the ball position and current of the actuator about the equilibrium position.
    - Reasonable: For the small signals we use, the relationship between these two variables does appear linear.
    - Violation to Assumption: As we try to navigate inputs further from equilibrium, our assumption will become less valid.
- Sensor(Emitter/Collector)
  - We assume the sensor subsystem contributes only a constant gain without dynamics. This is not exactly true but the assumption can be made because this subsystem is considerably faster than the others.
  - We are approximating the relationship between the output voltage of the collector and the position of the ball as linear about the equilibrium position. Reality is pretty close to this assumption, assuming we never hit the saturation voltages of the collector.

– We assume there is no bias voltage at the output of the op amp in the collector circuit. The bias would affect what we read as the quiescent voltage of the collector but it should be made negligible during calibration.

The assumption most likely to fail is the linearity of the sensor subsystem. This is because unlike with the op amp linearity assumption or the current-position linearity assumption, hitting the boundaries of the sensor linearity would cause the ball to fall or get stuck to the actuator, which is catastrophic. Whereas the op amp could saturate momentarily and the system would still be able to recover.

(b) Mathematical Model (3)

The overall Mag-Lev system can be divided into 5 separate subsystems:

- Actuator Driver
  To drive the electromagnet, the driver consists of a high-current power op-amp, OPA547T, that has been configured as a voltage-to-current amplifier. The voltage is supplied by the myRio into the system and the actuator driver provides current to the electromagnet.
  $$i_M = \left(\frac{R_2}{R_1 + R_2}\right)\left(\frac{1}{R_s}\right)e_{in} \tag{1}$$
  where i_M is the current through the electromagnet, R is the resistor, and e_{in} is the voltage entering the system.

- Electromagnet-Ball System
  This subsystem represents the interaction between the electromagnet and the ball. The ball has electromagnetic force acting upwards and gravity acting downwards. The equilibrium of this subsystem is defined by
  $$m\ddot{x} = mg - C\left(\frac{i^2}{x^2}\right) \tag{2}$$
  where m is the mass of the ball while x is the displacement of the top of the ball from the electromagnet, downward direction being positive. The i is the current flowing in the electromagnet. C is a property of the physical Mag-Lev system and compensates for all the assumptions made while deriving Eq. 2.

- Ball to Detector
  To detect the ball's position, the system has an photo-detector installed on the stand that senses the amount of light received from the photo-emitter. The position of the ball is transmitted as voltage through the detector. The relationship is
  $$e_{out} = K_s x + y_s \tag{3}$$
  where e_{out} is the output voltage read by the myRio, K_s is the sensitivity gain, and y_s is the voltage intercept of this relation. The sensitivity gain and voltage intercept are derived experimentally, which will be defined in later sections.

- Feedback Controller
  The system maintains the position of the ball at equilibrium by using a feedback controller. The difference between the commanded position and the actual position is represented by $\hat{x}$ and the voltage required to fix the position, $\hat{e}$ is found through

$$\frac{\hat{e}}{\hat{x}} = -\frac{K_D}{\tau} \cdot \frac{s + \frac{K_P}{K_D}}{s + \frac{1}{\tau}} = \frac{K(s+z)}{s+p} \tag{4}$$

  where K_D is the derivative gain, τ is the time constant, K_P is the proportional gain, K is the controller gain, z is the controller zero and p is the controller pole.

- Sensor Circuit
  The photo-emitter sends infrared light to the photo-detector to determine the position of the ball. The photo-emitter sends infrared light so that the ambient light does not affect data collection. The relationship between the emitter and the detector is given by

$$\frac{e_{photoemitter}}{e_{photodetector}} = 1. \tag{5}$$

(c) Block Diagram (3)

The control system is represented as a block diagram in Figure 1. This block diagram shows the conceptual closed-loop system. In reality, throughout this experiment, instead of position input, command voltage is inputted into the PD/Lead Controller and the voltage from the low pass filter is compared to the command voltage to determine the voltage difference between expected and actual.

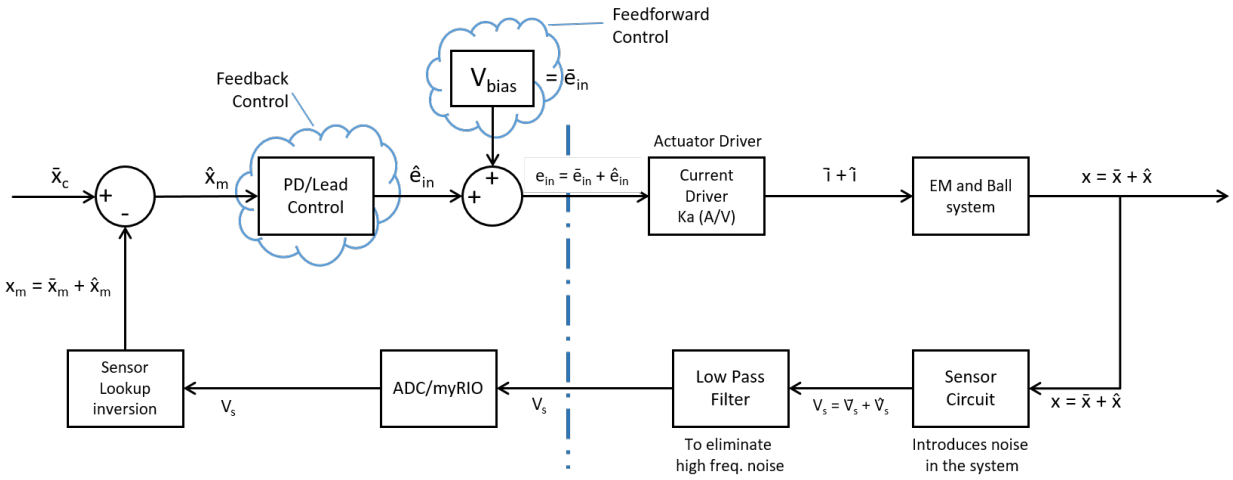

Figure 1: Block diagram of the overall system. The command position $\bar{x}_c$ is fed into the system, which results in a calculated position of the ball with respect to the system dynamics. The measured position is then fed back into the loop to compensate for the error in the desired position relative to the command position.

(d) Bias Voltage (3)

The bias voltage is the voltage needed to maintain equilibrium between the magnetic force of the actuator and the force of gravity on the ball. The voltage is used to preemptively counteract the force of gravity, and therefore is considered feed-forward control. The bias voltage is necessary for our control system because it provides the point around which we linearize the model, so that we can use our LTI assumptions.

(e) Driver (5)

The analog output of LabView VI is connected to the power amplifier circuit and its saturation limits would be dependent on the maximum current in the coil of the electromagnet. The magnet wire used in the experiment is 26 gauge and can handle maximum of 0.361A [1].Thus, using Eq. 1, the saturation limits should be 1.73V.

The polarity of the electromagnetic coil cause the current to run forward or backwards in the coil. Depending on the polarity, the electromagnet's magnetic field will change direction.

The OPA547T datasheet indicates that the output current limit range is $\pm$750 mA. The power supply used in the electromagnet circuit maximum current output is 2.2A. If the op-amp were to fail and become a short circuit, it may be possible that the maximum current of 2.2A of the power supply is directed into the electromagnet. To decided on the current limit of the magnetic coil, not only should we consider the current required to produce desired electromagnetic force but also the duration of the operation. As the operation time increases, the coil heats up, its limiting factor would be when the wire reaches its melting temperature.

2 Hardware and System ID (18pts)

(a) Sensing Scheme (9)

From data we took measuring the voltage produced by the sensor circuit as a function of the ball position, we found that across the full range of the relationship the relationship is non-linear. The non-linearity takes the form of saturation at the upper and lower bounds of the collector voltage. Despite this non-linearity, it is still possible to use the sensor across its entire voltage range with the use of a look-up table. A look-up table would be able to convert the output voltage of the sensor to a position value to be compared to a command position. A look-up table does not provide a linear relationship between the input and output however and so it would not be able to be modeled directly with linear controls theory(???)

A buffer is added to the collector circuit to ensure that there is no loading effect on the collector caused by the myRio. If there were a loading effect, then we would also have to take the power consumption function of the load across the sensors use range which would be

adding an unnecessary analytical hurdle. Removing the buffer would not make a difference to the system. This is because the inputs of the myRio are effectively op-amps themselves and so they already provide buffer functionality.

From the data sheet of the emitter, we know that the maximum continuous current through the emitter should be 100mA and the forward voltage is 1.2 Volts. We intend to supply 15V to this subsystem and therefore need to drop 13.8 of those across the resistors. Using

$$V = IR \tag{6}$$

where I is the max continuous current, V is equal to 13.8V and R is the resistor value we would like to find, we find that

$$\begin{aligned} 13.8V &= 0.1A * R \\ R &= 138\Omega \end{aligned} \tag{7}$$

The minmum resistance that we can use is 138Ω. If the resistance is too low, the emitter can overheat and die. If the resistance is too high, the emitter won't turn on.

(b) Linearization (5)

The Electromagnet + Ball sub-system (plant) is the only other non-linear aspect in our *simplified* Maglev model besides the sensing scheme and is represented by Eq. 2. Linearization of the nonlinear model is performed about an equilibrium (current $\bar{i}$ and ball position $\bar{x}$) condition chosen as the operating point for the system. Using Taylor series expansion about ($\bar{i}$, $\bar{x}$) and imposing $mg = C\left(\frac{\bar{i}^2}{\bar{x}^2}\right)$, we obtain the below shown linear model,

$$m\ddot{\hat{x}} \;=\; C\left(\frac{2\bar{i}^2}{\bar{x}^3}\right)\hat{x} \;-\; C\left(\frac{2\bar{i}}{\bar{x}^2}\right)\hat{i} \tag{8}$$

$\hat{x}$ is the displacement of the ball from its equilibrium position $\bar{x}$, while $\hat{i}$ is the fluctuation in the equilibrium electromagnet current i_M. Combining linear models for the current amplifier gain, plant and photodiode sensor gain, we get the following mathematical model for the *overall* physical system,

$$\hat{i} = K_a \hat{V}_{quiescent} \tag{9}$$

$$m\ddot{\hat{x}} \;=\; C\left(\frac{2\bar{i}^2}{\bar{x}^3}\right)\hat{x} \;-\; C\left(\frac{2\bar{i}}{\bar{x}^2}\right)\hat{i} \tag{10}$$

$$\hat{V}_{sensor} = K_s \hat{x} \tag{11}$$

The overall linear time invariant (LTI) transfer function for the system between $\hat{V}_{quiescent}$ and $\hat{V}_{sensor}$ can be given as

$$\frac{\hat{V}_{sensor}}{\hat{V}_{quiescent}} = (K_a)(K_s)\left(\frac{\frac{-2C}{m}\frac{\bar{i}}{\bar{x}^2}}{s^2 - \frac{2C}{m}\frac{\bar{i}^2}{\bar{x}^3}}\right) \tag{12}$$

(c) Parameter Identification (4)

From Eq. 6, we see that K_a, K_s, C and m are the quantities to be determined via parameter identification. They were identified as follows :

Mass of the ball m was measured using a digital weighing scale.

Photo-diode sensitivity K_s was measured by recording photodiode sensor voltages for different ball positions x, starting from the highest position of the stand, to its lowest. For every 1/6th turn of the hexagonal nut, the photodiode sensor voltage V_{sensor} was noted, resulting in a plot (Fig. 2) for V_{sensor} vs x using the knowledge that the screw moving the stand was a 1/4" - 20. The reading closest to the centre of the linear region was chosen as the equilibrium operating point of our system. Hence, we obtained $\bar{x}$ as 0.004 m and $V_{quiescent}$ as 6.873 V. Linearization about this point gives us a straight line relating V_{sensor} and x, the slope of which is K_s.

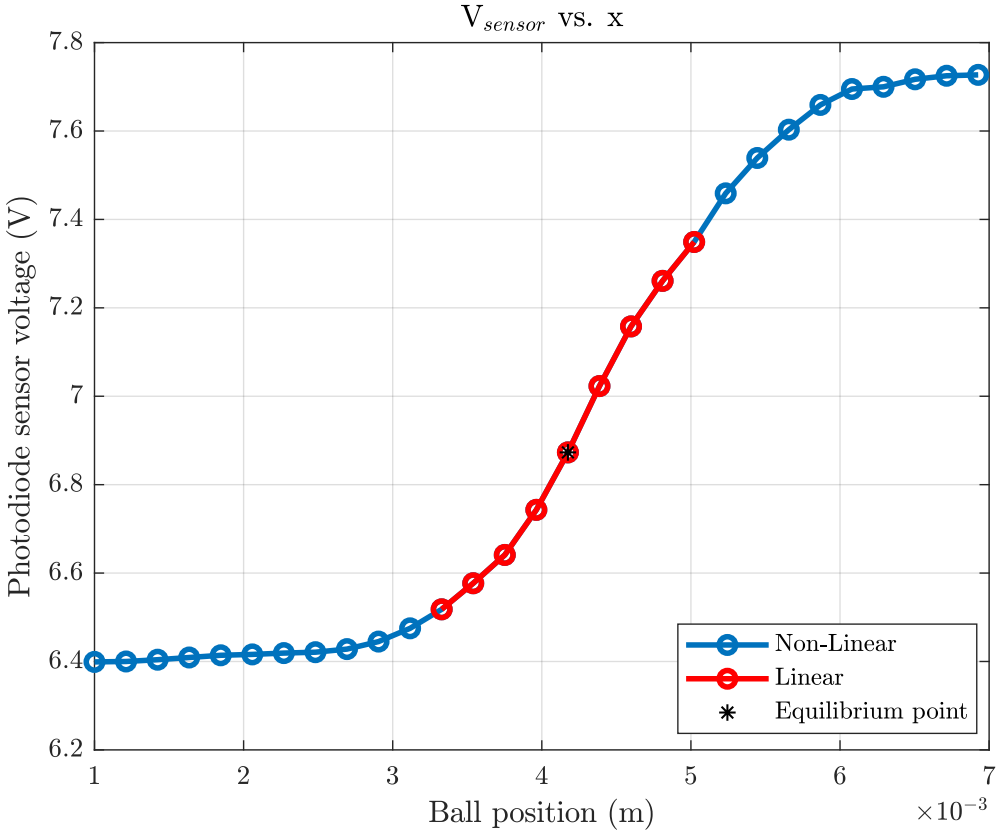

Figure 2: Photo-diode sensor voltage with respect to ball position. Linearizing about $(\bar{x}, V_{quiescent})$, we obtain the relation $V_{sensor} = 526.77x + 4.7$ (V) for our linear model.

The current amplifier gain K_a was obtained at the time of setting the equilibrium operating condition $(\bar{i}, \bar{x})$ for the ball. $AI1^+$ and $AI1^-$ myRio ports were used to measure the voltage across the 0.1 Ω sense resistance in the current amplifier circuit. This provided $\bar{i}$, the electromagnet current at equilibrium. Using V_{bias}, K_a was determined using the transfer

function (Eq.) for the current amplifier.

Table 1: Parameter Identification for the simplified Maglev physical model

Parameters	Value
K_a (A/V)	0.127
m (kg)	0.008
K_s (V/m)	526.77
C (N-m^{2}A^{-2})	1.7x10^{-5}

3 Simulation (21)

(a) Modeling in Simulink (16)

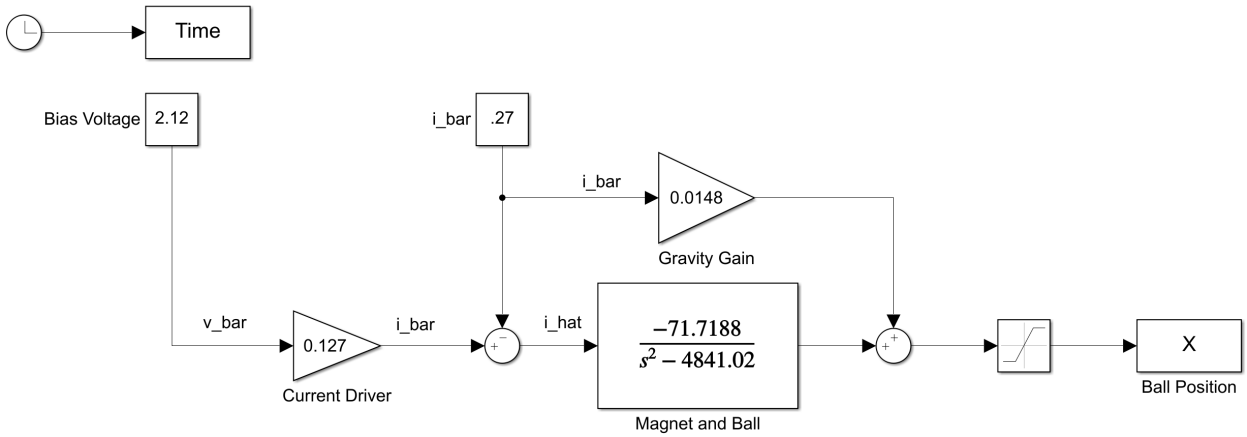

Figure 3: Simulink Block Diagram of Linearized Model without Controller

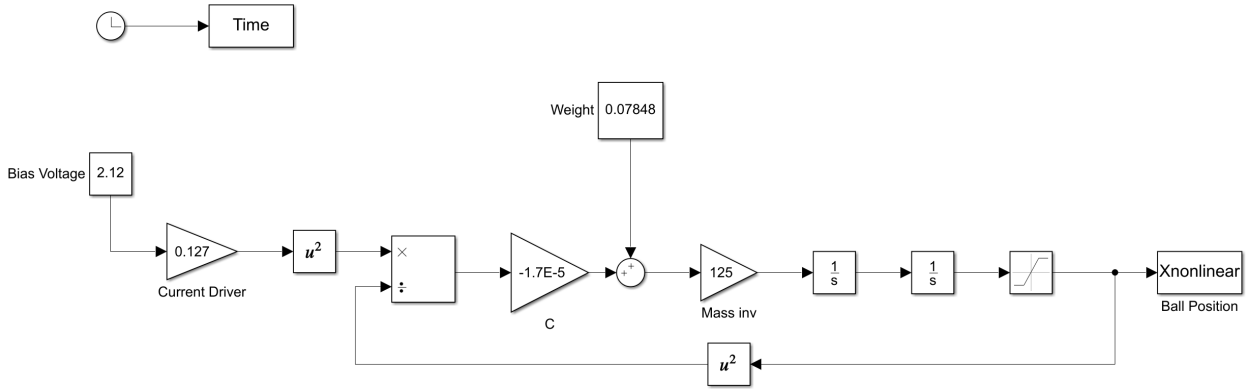

Figure 4: Simulink Block Diagram of Nonlinear Model without Controller

(b) Linear/Non-linear Model Comparison (5)

To compare the linear and nonlinear model of the magnetic levitation system, three different initial conditions were tested. Considering that the positive ball displacement is downward and away from the magnet, the models were tested for when the ball's initial position is at equilibrium (4mm), above equilibrium (8mm), and below equilibrium (2mm) as shown below. The displacement range of the ball is limited by the electromagnet (0mm) and by the base of the stand (10.4mm).

When the ball is dropped from equilibrium, it is expected that the ball would maintain the position. However, due to the precision limitations from experimental constants, if the system does not have a controller, the magnetic levitation system is not able to hold the ball in equilibrium. This behavior is seen in Figure 5. The system seem to be able to maintain the equilibrium position at the very beginning; however, as the ball displaces further from equilibrium, the system is unable to control the ball and the nonlinear and linear model predictions begin to deviate. Additionally, although the figure illustrates that the nonlinear model predicts the ball to drop faster at the beginning, the linear model predicts the ball to land on the base of the stand earlier. Similarly, when the ball's position was set to be above equilibrium, the ball drops to the base. Figure 6 show that since the ball was set at a further location from the equilibrium, the relative stability seen in Figure 5 has been shortened and the nonlinear and linear model predictions deviate from each other faster. As well, the linear model again predicts the ball to drop faster to the base. On the other hand, when the ball's initial position is set to below equilibrium, the ball is attracted to the electromagnet and decreases in position and sticks to the electromagnet. Unlike the previous graphs, Figure 7 show that the nonlinear model predicts the ball to arrive at the electromagnet first and the two models deviate almost instantaneously.

The magnetic levitation system dynamic modeling was able to the linearized with the assumption that the electromagnetic force will be linear about the equilibrium point. This allows us to assess the local stability of the equilibrium point of the nonlinear dynamic system. However, as the ball diverges further from the equilibrium point, the linearization assumption becomes less effective. When the ball is displaced above the equilibrium, the linear model predicts faster drop than the nonlinear model, while when the ball is displaced below the equilibrium, the linear model predicts slower attraction to electromagnet than the nonlinear model. Thus, linearized electromagnet force is smaller in magnitude than the nonlinear electromagnet force. The linearized electromagnet force is only truly effective near the equilibrium point.

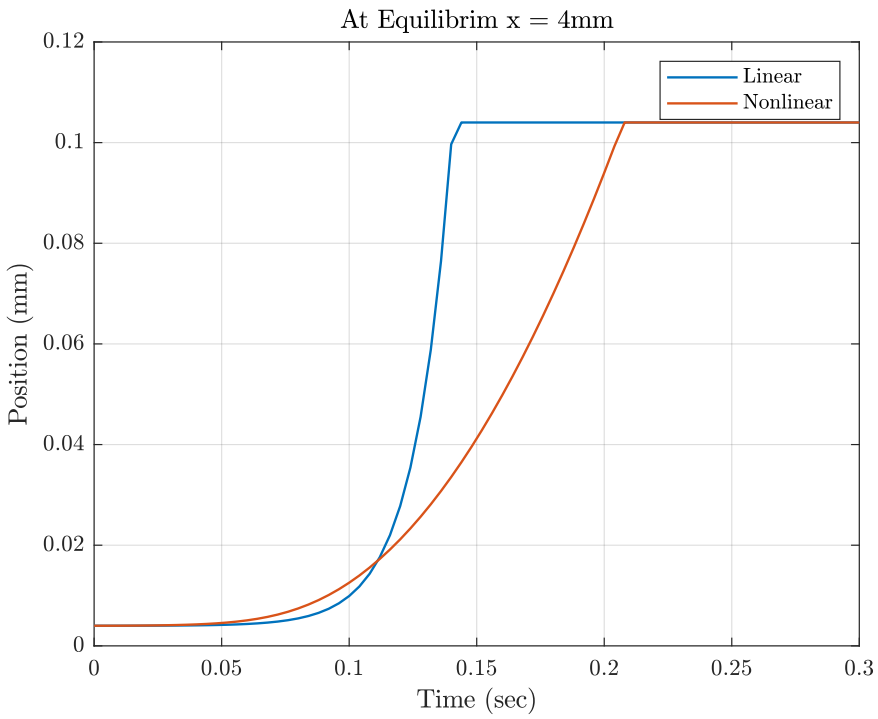

Figure 5: Ball's Displacement with Initial Condition at Equilibrium. The linear and nonlinear model predicts the ball to drop to the base of the stand. Although at the beginning of the drop, the nonlinear model predicts the ball to drop faster, as time increases, the linear model has a higher slope and predicts the ball to fall on the base before the nonlinear model.

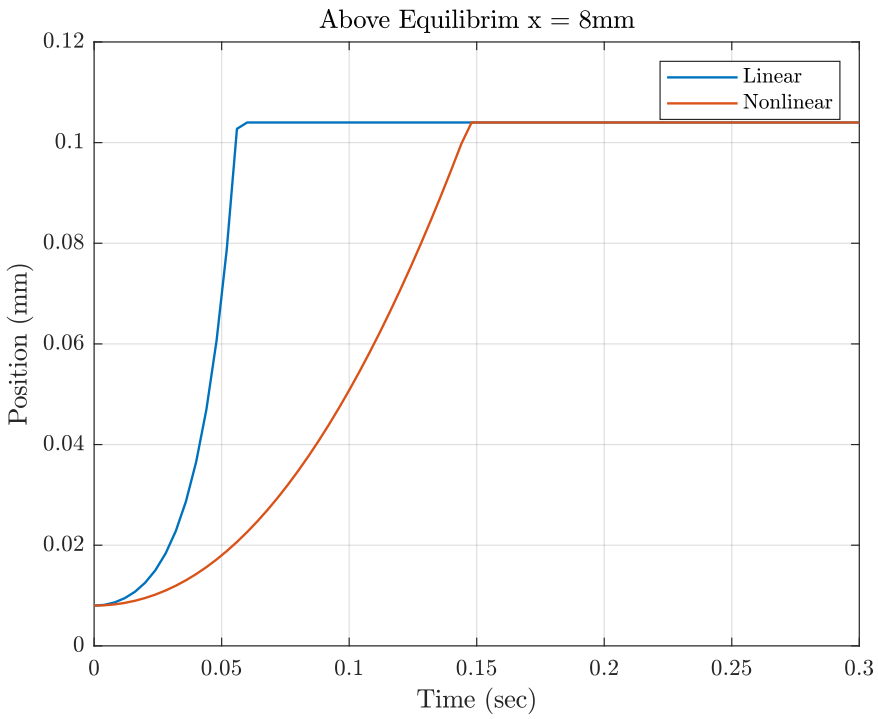

Figure 6: Ball's Displacement with Initial Condition at Above Equilibrium. The linear model predicts that the ball would drop faster than the nonlinear model.

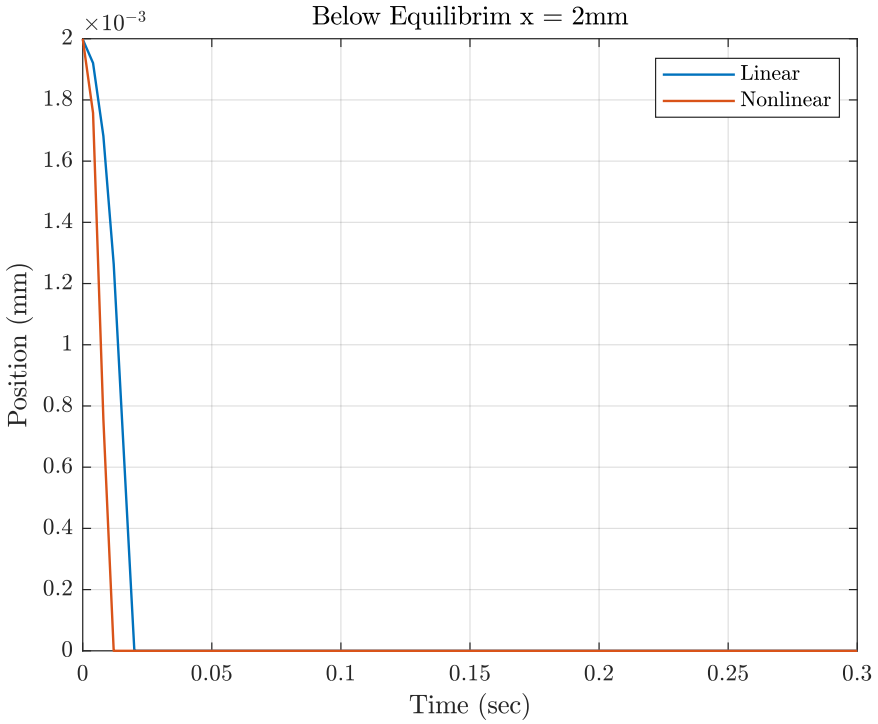

Figure 7: Ball's Displacement with Initial Condition at Below Equilibrium. The nonlinear model predicts that the ball would touch the electromagnet faster than the linear model.

4 Control System Design (20)

(a) Sign Convention (3)

The Maglev system block diagram was further simplified for the purposes of controller design.

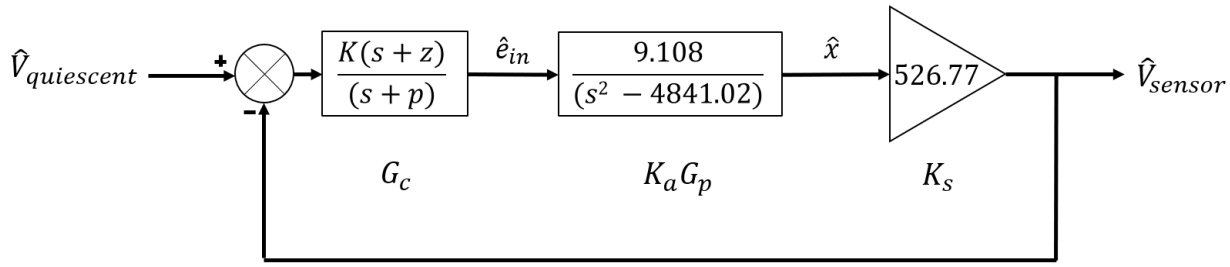

Figure 8: The simplified Maglev closed loop LTI system in unity feedback.

A simplified block diagram of the system, shown in Fig. 21, primarily contains three subsystems, i.e the controller block (G_C), the plant ($K_a \cdot G_P$) and the sensor block (K_S). Each of the blocks have a positive transfer function, and a unity feedback with a negative sign in the summing block, ensures the negative feedback for the overall closed loop. [WHAT ELSE CAN BE ADDED??]

(b) Controller Design (12)

A change in command voltage $\hat{V}_{quiescent}$ leads to a change in ball position which must be reflected in the photo-diode sensor voltage $\hat{V}_{sensor}$. G_c is the lead controller which produces a correcting voltage input $\hat{e}_{in}$. K_aG_p represents the combined transfer function for the current amplifier and electromagnet + ball subsystems and determines the change in ball position $\hat{x}$. K_s is the photodiode sensitivity gain that outputs a $\hat{V}_{sensor}$.

In the absence of a controller, the open loop transfer function $K_aG_pK_s$ has complex roots and one of the roots is on the real axis in the s plane and is therefore unstable. The lead controller design was initiated with the aim of having two dominant poles for the closed loop system in unity feedback. Preliminary analysis using *sisotool* showed that a stable system will have a natural frequency ω_n of the order of hundred radians per second. Hence, a target $\omega_n = 200$ rad/s and (arbitrary) damping ratio $\zeta = 0.8$ was chosen.

Using traditional pole placement techniques (angle and magnitude criterion for a closed loop pole on a root locus plot), we obtain $z = 86.26$, $p = 463.55$ and $K = 19$. The theoretical controller transfer function is

$$G_c = \frac{19(s + 86.26)}{s + 463.55}. \tag{13}$$

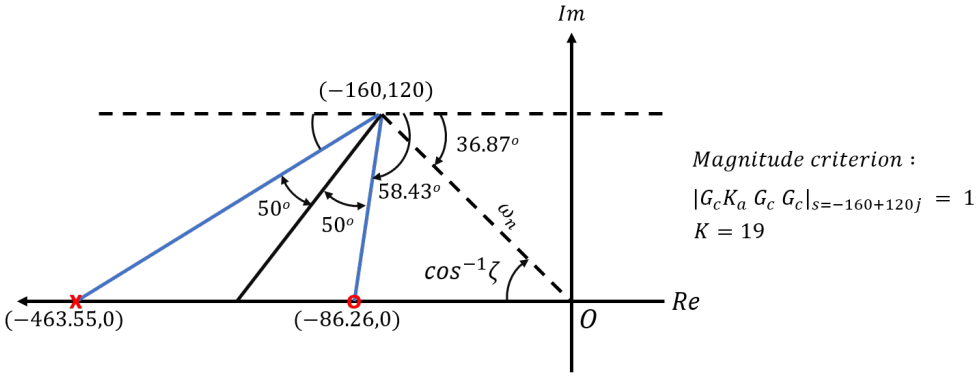

Figure 9: Pole Placement Diagram. Based on the frequency and damping requirements, the dominant closed loop poles were required at $s = -160 + 120j$. An angle deficiency of 100^o in open loop is compensated for by adding a pole and zero in closed loop.

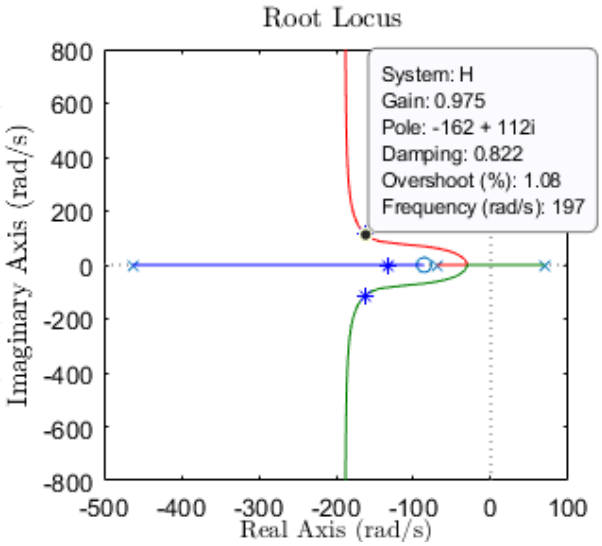

Figure 10: Close Loop Root Locus Plot

As can be seen from the root locus plot, with the present controller an open loop gain of 0.97 is obtained. The root locus will never cross the imaginary axis on raising the gain further. Hence it can be said that the system has an infinite gain stability margin.

The closed loop transfer function for the overall system can be given as

$$G = \frac{G_c K_a G_p K_s}{1 + G_c K_a G_p K_s} = \frac{(91158.6)(s + 86.26)}{(s^3 + 464.55s^2 + 86317.6s + 5593406.5)} \tag{14}$$

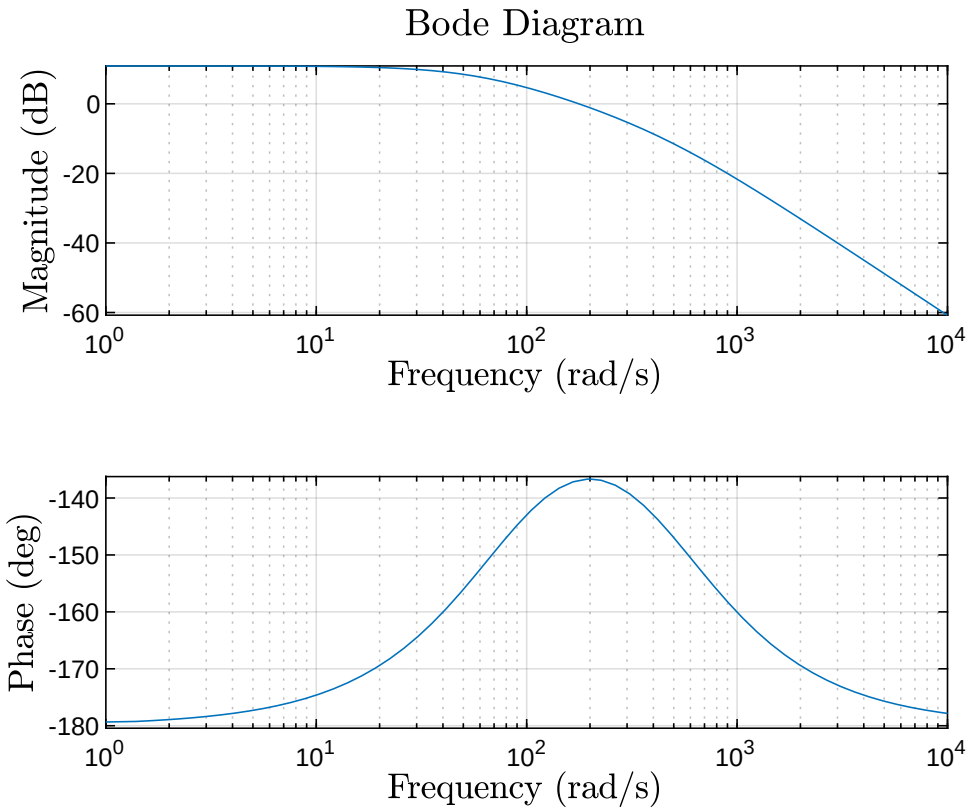

Figure 11: Closed Loop Bode Plot

Based on the Bode plot we expect a closed loop bandwidth of $\sim$ 390 rad/s in theory.

(c) Controller Performance Simulation (5)

The above mentioned controller is then implemented in the linear and non-linear Simulink model, shown in Fig. 12 and Fig. 13.

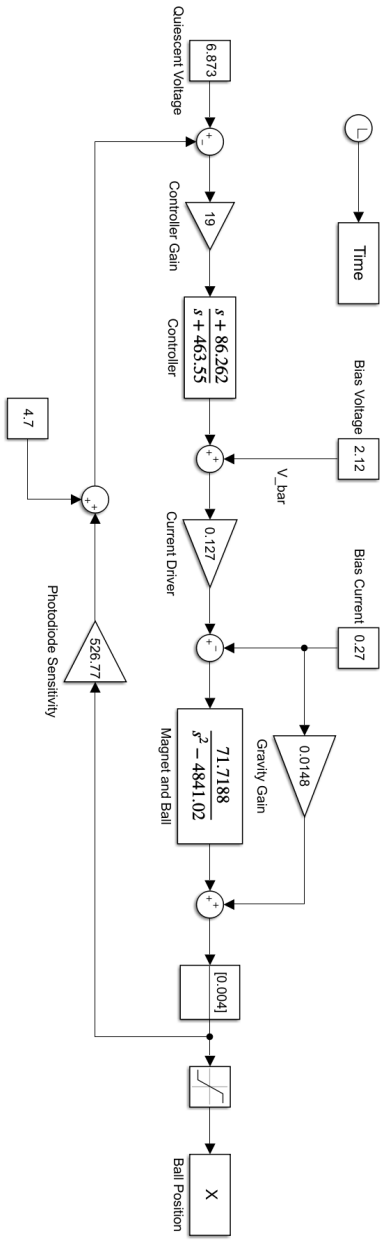

Figure 12: Complete Simulink model of the Linear system with controller design.

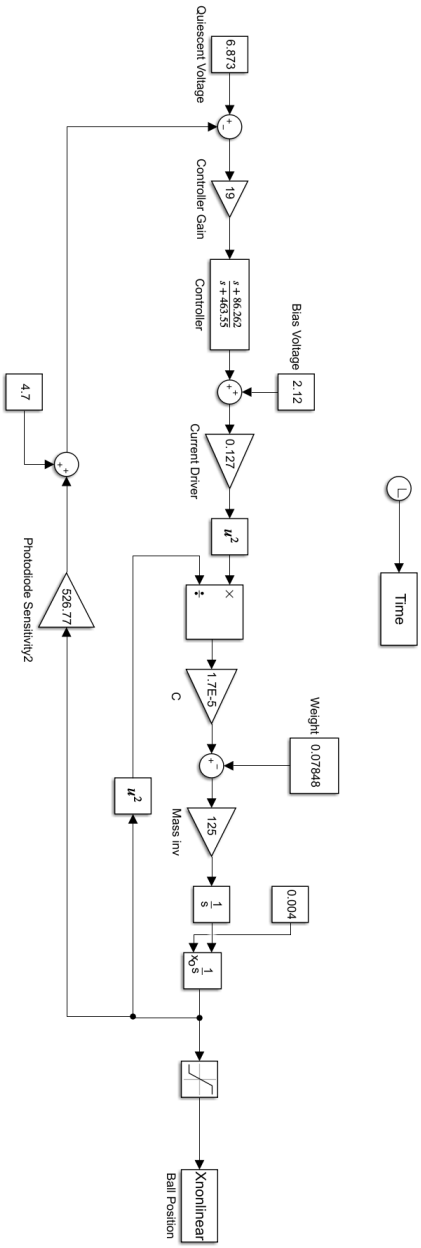

Figure 13: Complete Simulink model of the Non-Linear system with controller design.

To demonstrate the closed loop response of the system, both the models are first deviated slightly from the equilibrium point and then the deviation is increased to a point when the system becomes unstable. As shown in Fig. 14 and Fig. 15, the system responds robustly when the ball is slightly deviated from the equilibrium position. But the closed loop response is not same for both the models when the starting position of the ball is increased. In case of the linear system (Fig. 16), the ball still stabilizes at the equilibrium position even if the ball is deviated by 10 mm which is the maximum the ball can move in the Maglev system. The maximum deviation observed in case of the non-linear system (Fig. 17) is 4.805 mm, after which the system becomes highly unstable.

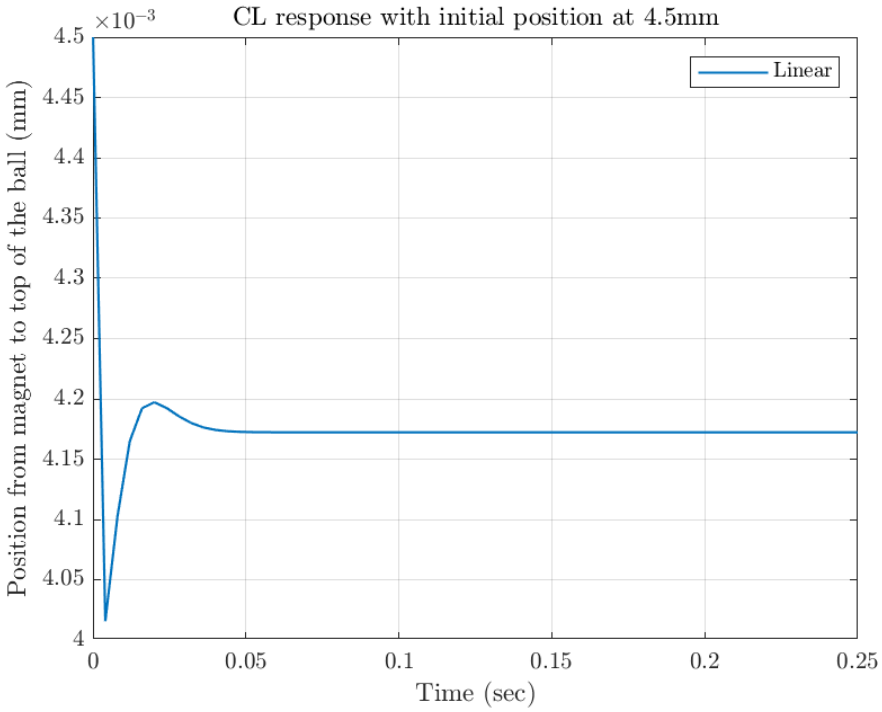

Figure 14: Closed loop response of the linear system when the ball is slightly deviated from the equilibrium position by 4.5mm.

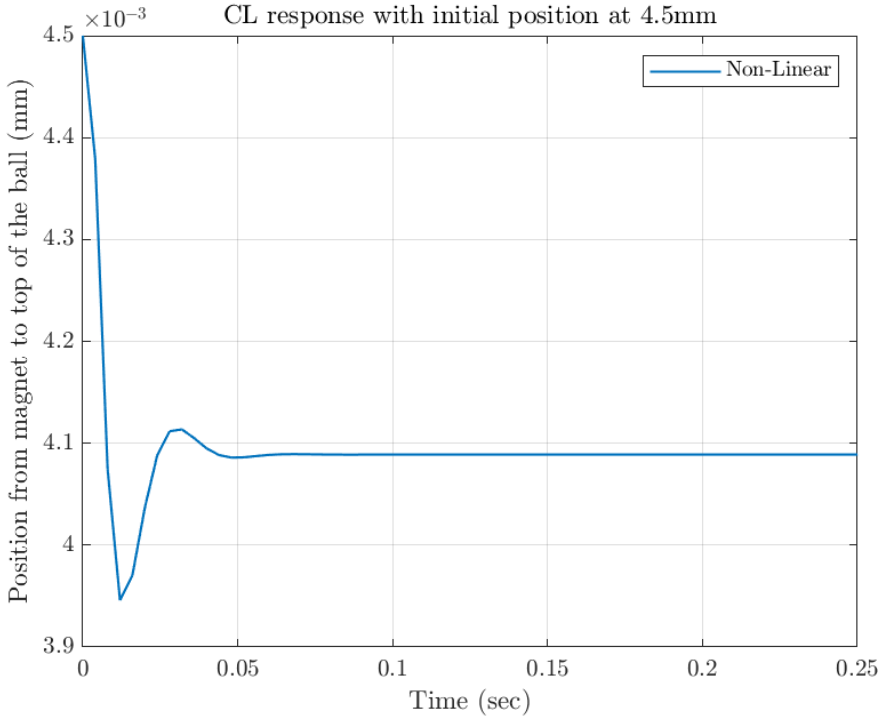

Figure 15: Closed loop response of the non-linear system when the ball is slightly deviated from the equilibrium position by 4.5mm.

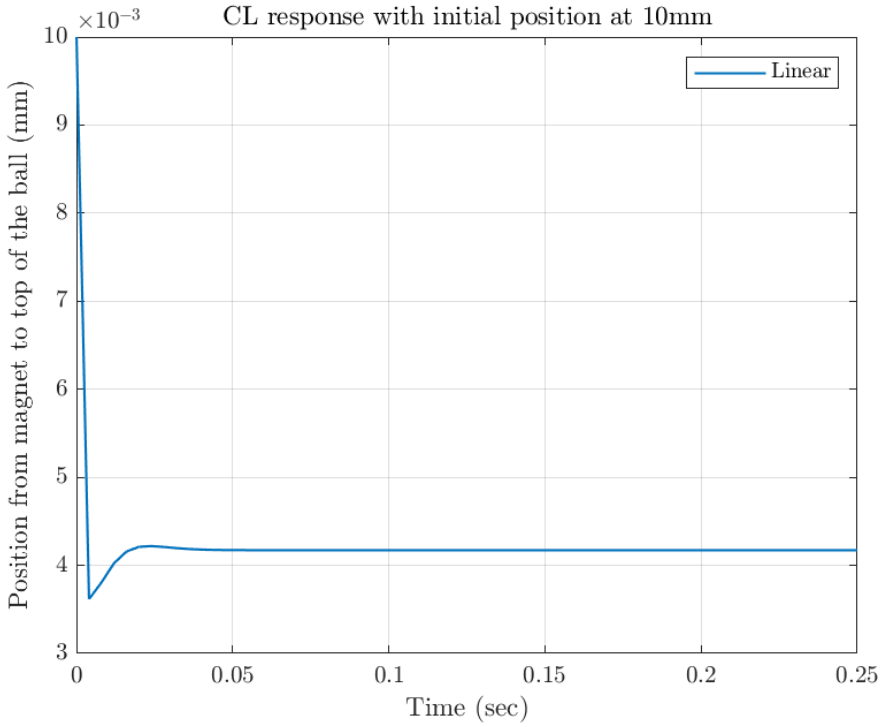

Figure 16: Closed loop response of the linear system when the ball is deviated by a large value of 10mm.

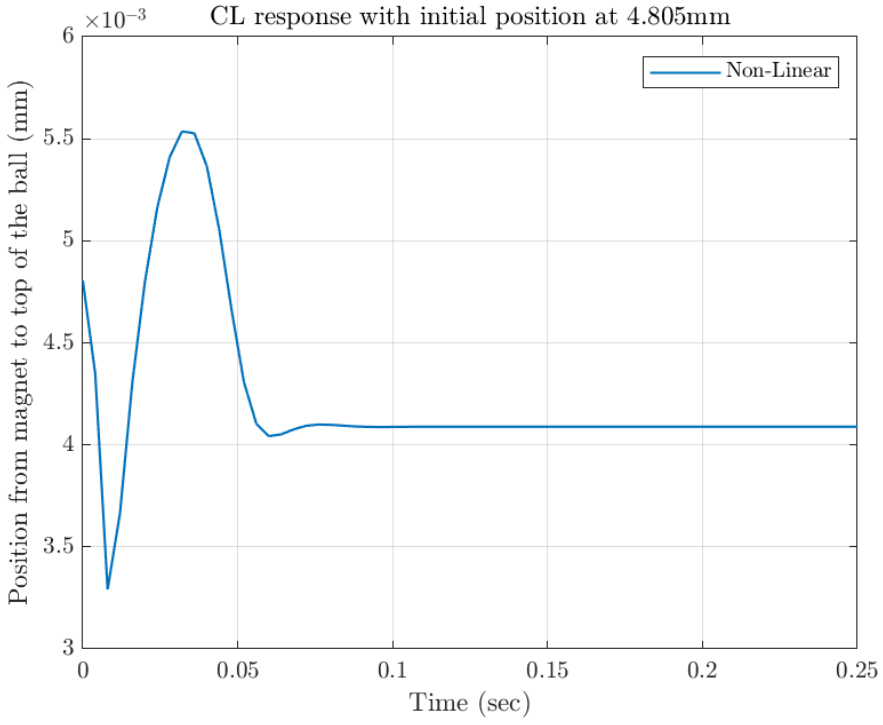

Figure 17: The final stable closed loop response of the non-linear system when the ball is deviated by a large value of 4.805mm.

Since the non-linear model is a close approximation of the real model, the final steady state value in case of the non-linear model is closer to the experimental equilibrium point, i.e. 4 mm. Whereas, introducing major disturbances in the linear model is perfectly compensated by the controller, resulting in less peak overshoot, less rise time and less settling time.

5 Experiments (39)

(a) Controller Implementation (10)

Controller on the hardware is given by Eq. 15

$$C(s) = \frac{10s + 1800}{s + 463.5} \tag{15}$$

The controller equation in K_P, K_D and τ can be expressed as:

$$C(s) = \frac{3.883 + 0.0215s}{0.002s + 1} \tag{16}$$

where, $K_P = 3.883, K_D = 0.0215$ and $\tau = 0.002$

The experimentally tuned controller gain values given by the Eq. 15, resulted in the stabilized levitating ball (Fig. 18)

Figure 18: Levitated ball in the maglev system.

(b) Experiment vs. Simulation (6)

The theoretical model of the controller defined by the Eq. (13) when implemented in the real model resulted in low response to error and a high noise accumulation in the system (increased oscillations in the magnet ball system). In order to make the controller more robust and thus to increase its performance, the proportional gain was increased which in turn increased the response of the system to disturbances; and the derivative gain was decreased, which decreased the oscillations of the ball in the equilibrium point.

There are significant observable differences when the experimental controller gain values are implemented on the linear and non-linear Simulink model. Since the proportional gain was increased, the rise time decreased slightly, but the overshoot increased significantly. Because of a rise in the peak amplitude and the derivative gain being decreased from the theoretical value, there are increased oscillation in the time response, which results in high settling time. The observations mentioned are similar for the linear model (Fig. 19) and the non-linear model (Fig. 20).

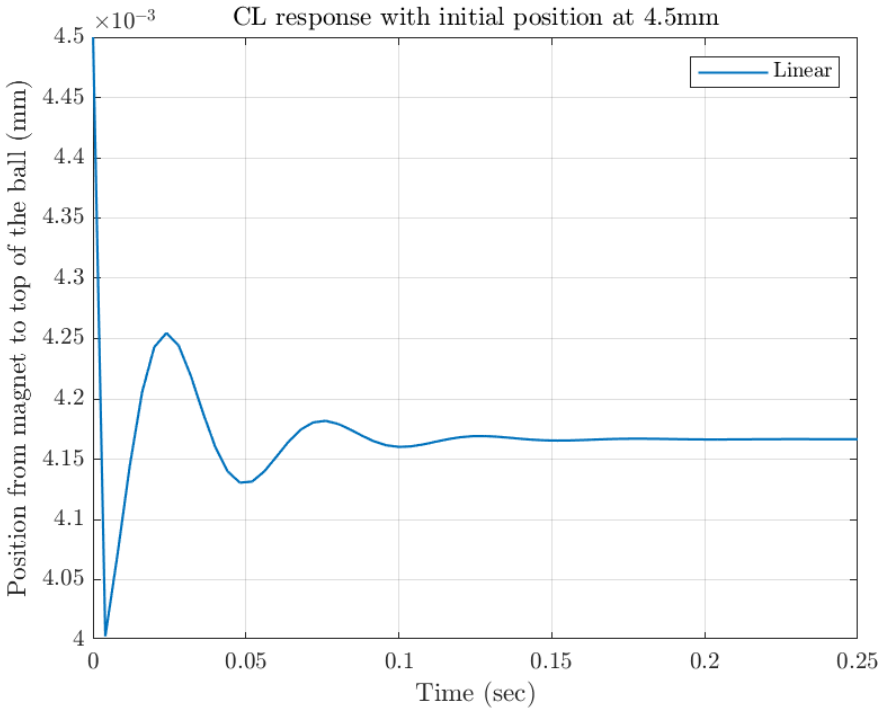

Figure 19: Closed loop response of the linear system, with the experimentally obtained controller gain values; when the ball is slightly deviated.

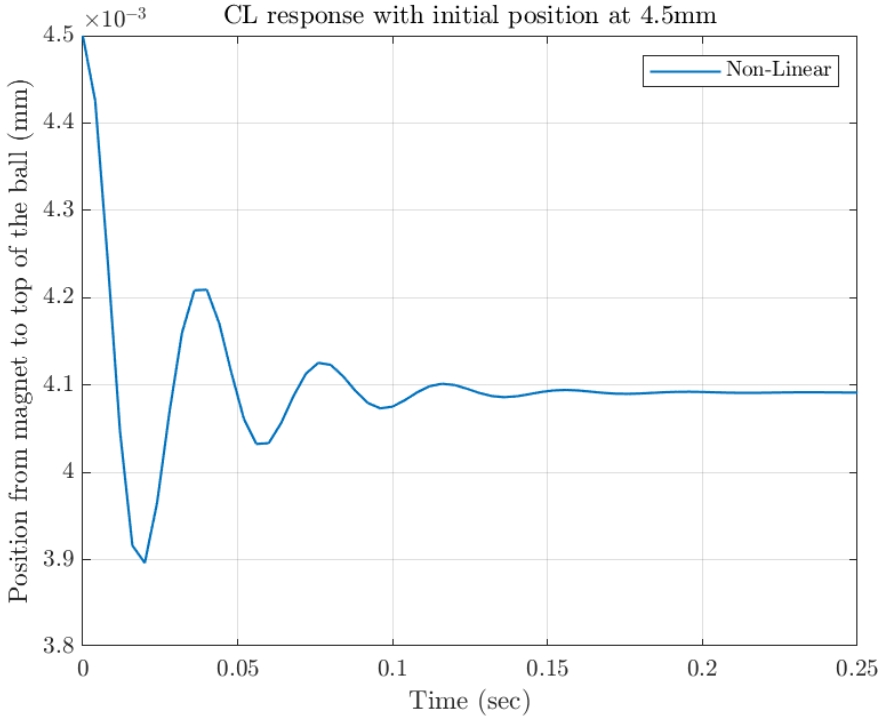

Figure 20: Closed loop response of the non-linear system, with the experimentally obtained controller gain values; when the ball is slightly deviated.

(c) Range of Operation (6)

The range of $V_{command}$ where the system can maintain and control the ball position for given value of V_{bias} is shown in Table 2. Outside of these limits, the ball would either stick to the electromagnet or would drop to the base of the stand. Additionally, the range of $V_{command}$ was also found theoretically using the linear and nonlinear block diagrams shown in Table 3. The experimental observation matches relatively well with the nonlinear model range as the lower limit difference is 0.4% and the upper limit difference is 1.4%. On the other hand, the linear model does not match the experimental observation well. The difference in the limit values are maximum 2V; however, this value was limited by the operation range. The linear model predicts that no matter what the quiescent voltage, it would be able to stabilize and control the ball position due to the limitations of the linear approximation and also due to the limitation of the system components have not been considered. As previously mentioned, the linear model predictions are only valid near the equilibrium as the electromagnet force has been linearized around the equilibrium point.

Table 2: Experimental range of $V_{command}$ as V_{bias} is held constant at 2.12V

Lower Limit	Upper Limit
6.512 V	7.050V

Table 3: Theoretical Range of $V_{command}$ as V_{bias} is held constant at 2.12V. The limits were found at either when the system could no longer stabilize the system or when the ball's peak response hits the displacement range limit.

Model	Lower Limit	Upper Limit
Linear	6.480V	8.990V
Nonlinear	6.539V	7.150V

(d) Frequency Response (13)

Instead of a constant value for $V_{command}$, also known as $V_{quiescent}$, a sine signal with 0.05V amplitude and 6.873V DC offset was sent into the system. The frequency of the sinusoidal signal was increased incrementally until the ball stopped responding to the command input at 10.2 Hz and dropped onto the stand. Potential reasons for the system to stop responding to the command input may be due to the lag in the controller and plant. As the frequency of the input is increased, the ball begins to oscillate at higher frequency as expected; however, due to the lag in system components, the system may not be able to respond as fast as the change in position, causing a failure. It's response is shown in Figure 21 along with the overall closed loop system transfer function, similar to Eq. 14, but with experimental controller transfer function that had been varied in LabView. Comparing the experimental and theoretical bode plots, the magnitude bode plot shows a discrepancy between the theoretical

and experimental values, while the phase bode plot shows a smaller discrepancy between the two data. The discrepancy in the bode plots are mainly from the disturbances impacting the system, which were not considered in the theoretical closed loop transfer function. The system, in reality, sees driver noise, ground vibration and sensor noise. Specifically is the disturbance from the driver and ground are large in the forward path, the output voltage would be greater than expected.

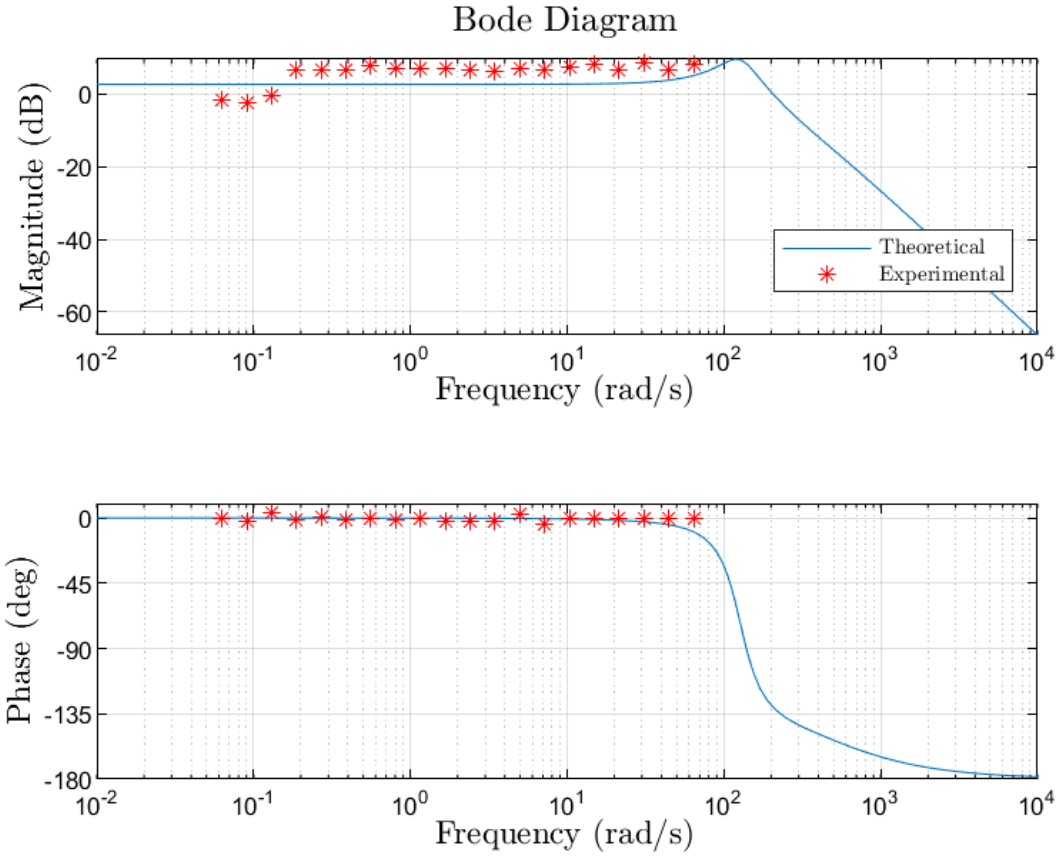

Figure 21: Bode plot of a sinusoidal input with 0.05V amplitude and 6.873 DC offset. The experimental values were measured until the ball stopped responding to the input and dropped onto the stand.

(e) Robustness against Bias Voltage (4)

The experimental range of the V_{bias} where the ball position is maintained or controlled is shown in Table 4. The range represents the controller robustness against modeling error in feed-forward controller design.

Table 4: Experimental range of V_{bias} as $V_{command}$ is held constant at 6.873V

Lower Limit	Upper Limit
1.41V	3.53V

6 Revisit Controller Design (9)

(a) Potential Controller Design (3)

Theoretically, the proposed controller C_1(s)=K$_P$ + K_Ds = K(s+z$_1$ will not perform the same as our controller, C_0(s)=K$\frac{s+z_1}{s+p_1}$. This is because the proposed controller lacks the high frequency pole which attenuates high frequency noise. In a practical context, the proposed controller may indeed perform similarly. This is because the PD controller cannot provide the same noise attenuation as the lead controller, due to the lack of a high frequency pole. Practically speaking, myRios sampling rate of about 50 kHz acts as a low pass filter in itself and so it is possible that the PD controller has a similar performance as the lead controller, but it would depend on what frequency the lead controller starts attenuating. The answer would be the same even if the myRio sampled at 1MHz. There will be a set of configurations where the performance is the same. Even for a controller made of op amps, resistors and capacitors, there will be a point where a PD controller acts the same as a lead controller because the op amp itself has a bandwidth that will attenuate the signal at high enough frequencies.

(b) PID Controller (3)

The proposed PID controller $C_2(s) = \frac{K_P+K_I/s+K_Ds}{s+p_1} = K\frac{(s+z_1)(s+z_2}{s(s+p_1)}$ will not better stabilize the ball compared to our original controller. This is because the added pole at s=0 forces the break-out point of the root locus to be on the right-hand side of the s-plane. This gives the controller much less potential to bring the closed-loop poles to the left-hand side, a prerequisite of stability. For many open-loop zeros of the system it won't be possible at all. The advantage of this controller would be less steady state error than our current configuration.

(c) Increasing Loop Gain (3)

Increasing loop gain in a system like ours can lead to a few side effects. The first of which is that due to the system having more poles than zeros, increasing the gain will decrease the damping and consequently increasing the overshoot and settling time. As the gain increases, the phase margin will also drop closer and closer to $\angle$180. At some point, the phase margin could become low enough that unmodeled dynamics bring the system to instability. Secondly, an increased loop gain could also increase the chance of saturating the current driver. In any case, a higher gain value would increase the power draw of the system which would increase the heat production of the system which in some contexts may be undesirable.

7 References

References

[1] Magnet Wire Current. (2012). Retrieved from http://www.magnetwire.biz/magnet_wire_current.html

Appendix A: Source Code

Listing 1: MATLAB code for computing linear and nonlinear model displacement prediction plots.

```
%%MECHENG 552 - Lab2
%%Author: Ellen Kim

clc; clear; close all;

load Linear_eq
eqLt = out.tout;
eqLx = out.X.Data;

load NonLinear_eq
eqNLt = out.tout;
eqNLx = out.Xnonlinear.Data;

load Linear_aboveeq
aboveLt = out.tout;
aboveLx = out.X.Data;

load NonLinear_aboveeq
aboveNLt = out.tout;
aboveNLx = out.Xnonlinear.Data;

load Linear_beloweq
belowLt = out.tout;
belowLx = out.X.Data;

load NonLinear_beloweq
belowNLt = out.tout;
belowNLx = out.Xnonlinear.Data;

%Equilibrium
figure();
hold on
plot(eqLt,eqLx,'LineWidth',1);
plot(eqNLt,eqNLx,'LineWidth',1);
set(gca,'ticklabelinterpreter','latex');
xlabel('Time (sec)','interpreter','latex');
ylabel('Position (mm)','interpreter','latex');
title('At Equilibrim x = 4mm','interpreter','latex');
legend({'Linear','Nonlinear'},'interpreter','latex');
% xlim([0 0.1]);
box on
grid on
hold off
```

```
tightfig();
saveas(gca,'Eq.pdf');

%Above
figure();
hold on
plot(aboveLt,aboveLx,'LineWidth',1);
plot(aboveNLt,aboveNLx,'LineWidth',1);
set(gca,'ticklabelinterpreter','latex');
xlabel('Time (sec)','interpreter','latex');
ylabel('Position (mm)','interpreter','latex');
title('Above Equilibrim x = 8mm','interpreter','latex');
legend({'Linear','Nonlinear'},'interpreter','latex');
% xlim([0 0.1]);
box on
grid on
hold off
tightfig();
saveas(gca,'Above.pdf');

%Below
figure();
hold on
plot(belowLt,belowLx,'LineWidth',1);
plot(belowNLt,belowNLx,'LineWidth',1);
set(gca,'ticklabelinterpreter','latex');
xlabel('Time (sec)','interpreter','latex');
ylabel('Position (mm)','interpreter','latex');
title('Below Equilibrim x = 2mm','interpreter','latex');
legend({'Linear','Nonlinear'},'interpreter','latex');
xlim([0 0.05]);
box on
grid on
hold off
tightfig();
saveas(gca,'Below.pdf');
```